



## Superior cycle performance of Sn@C/graphene nanocomposite as an anode material for lithium-ion batteries

Shuzhao Liang<sup>a</sup>, Xuefeng Zhu<sup>b</sup>, Peichao Lian<sup>a</sup>, Weishen Yang<sup>b</sup>, Haihui Wang<sup>a,\*</sup>

<sup>a</sup> School of Chemistry & Chemical Engineering, South China University of Technology, Wushan Road, Guangzhou 510640, PR China

<sup>b</sup> State Key Laboratory of Catalysis, Dalian Institute of Chemical Physics, Chinese Academy of Sciences, Dalian 116023, PR China

### ARTICLE INFO

#### Article history:

Received 15 December 2010

Received in revised form

24 March 2011

Accepted 29 March 2011

Available online 13 April 2011

#### Keywords:

Tin

Carbon coating

Graphene

Anode material

Lithium-ion batteries

### ABSTRACT

A novel anode material for lithium-ion batteries, tin nanoparticles coated with carbon embedded in graphene (Sn@C/graphene), was fabricated by hydrothermal synthesis and subsequent annealing. The structure and morphology of the nanocomposite were characterized by X-ray diffraction, scanning electron microscopy, and transmission electron microscopy. The size of the Sn@C nanoparticles is about 50–200 nm. The reversible specific capacity of the nanocomposite is  $\sim 662 \text{ mAh g}^{-1}$  at a specific current of  $100 \text{ mA g}^{-1}$  after 100 cycles, even  $\sim 417 \text{ mAh g}^{-1}$  at the high current of  $1000 \text{ mA g}^{-1}$ . These results indicate that Sn@C/graphene possesses superior cycle performance and high rate capability. The enhanced electrochemical performances can be ascribed to the characteristic structure of the nanocomposite with both of the graphene and carbon shells, which buffer the volume change of the metallic tin and prevent the detachment and agglomeration of pulverized tin.

© 2011 Elsevier Inc. All rights reserved.

### 1. Introduction

Lithium-ion battery is the most widely used rechargeable battery because of its high energy density and excellent service life. However, the energy density and power density of lithium-ion batteries still lies behind the demands of consumers. To improve the electrochemical performances of lithium-ion batteries many new electrode materials have been exploited to obtain such batteries with high energy density, long cycle life, as well as eco-friendliness [1–6]. Among the developed anode materials, metallic tin (Sn) is considered to be a promising anode material because of its high theoretical specific capacity of  $\sim 992 \text{ mAh g}^{-1}$ , which is much higher than that of the commercial graphite ( $372 \text{ mAh g}^{-1}$ ). However, the lithiation and delithiation reactions ( $\text{Sn} + 4.4\text{Li}^+ + 4.4\text{e}^- \leftrightarrow \text{Li}_{4.4}\text{Sn}$ ) are accompanied by a large volume change [7–9], which lead to the pulverization of the particles and the electrical disconnection of the electrode. This is the major reason for the poor cycle life of metallic Sn, which hampers the application in lithium-ion batteries [10,11]. Sn particles are usually prepared in nanoscale in order to improve the rate capability, since nanoscale metallic has high activity and short pathway for  $\text{Li}^+$  transport. Nevertheless, aggregation is a

general problem for nanoscale materials, especially in charge-discharge process in batteries.

Many efforts have been devoted to improving the electrochemical performance of metallic Sn such as carbon-coating, nanocomposite and porous structure [12–15]. Among the reported approaches, the cycle performance of Sn anode can be considerably improved using carbon matrixes to disperse nanostructure Sn. The carbon matrixes cannot only accommodate the volume change of Sn during charge–discharge process but also provide the electron transport pathways due to the high electronic conductivity of the carbonaceous materials. Various carbon matrixes with different morphologies have been used to prepare Sn/C composites, such as carbon nanotubes [16,17], carbon nanofibers [18], hollow carbon spheres [19,20], and carbon microbeads [21]. All these Sn/C composites show better cycle performance than bare Sn anode material.

Carbon shells coated on the nanoparticles can provide a buffer for the volume change and prevent the aggregation of the particles. However, the metallic Sn with only carbon shell reported previously still exhibited capacity fading [19] because the carbon shell is not elastic enough to compensate the large volume change of Sn. Graphene, a single-atom-thick sheet of honeycomb carbon lattice, was discovered in 2004 and proved to be chemically stable and possess excellent electron conductivity [22]. Graphene nanosheets (GNSs) should be an excellent carbon matrix for dispersing Sn as anodes with good cycle performance and high rate capability because of the natural structure of curly and wrinkled of the disordered stacked GNSs, which create

\* Corresponding author. Fax: +86 20 87110131.

E-mail addresses: [sz.liang02@mail.edu.cn](mailto:sz.liang02@mail.edu.cn) (S. Liang), [hhwang@scut.edu.cn](mailto:hhwang@scut.edu.cn) (H. Wang).

substantial void spaces. On the other hand, GNSs are more flexible than carbon shell due to the wide and open porous graphene base. Although the previously reported graphene-based tin anode material without carbon coating improved the cycle performance, the capacity slowly faded from 796 to about 500 mAh g<sup>-1</sup> even at a small specific current of 55 mA g<sup>-1</sup> [23]. In order to avoid detachment of the pulverized Sn particles, a novel Sn nanoparticles coating with carbon embedded in graphene (Sn@C/graphene) is proposed. Carbon coated on Sn can wrap up the pulverized Sn particles. Meanwhile, carbon coating is regarded as a conducting bridge between GNSs and Sn particles in the nanocomposite. Moreover, graphene-based Sn was normally prepared by reducing SnO<sub>2</sub>/graphene nanoparticles at 800 °C and carbon coating plays a special role, which protects the melting Sn from aggregation while reducing since the melting point of Sn is 232 °C. It can be expected that the as-prepared Sn@C/graphene nanocomposite with characteristic morphology as anode for lithium-ion batteries exhibits large reversible specific capacity, superior cycle performance and excellent rate capability.

## 2. Experimental

GNSs were prepared through the thermal exfoliation of graphite oxide, which was synthesized by a modified Hummers' method [24]. The detailed preparation process for the GNSs is described in our previous work [25]. SnO<sub>2</sub> nanoparticles aqueous colloid was obtained by fiercely stirring 35 mL of 0.0775 mol L<sup>-1</sup> SnCl<sub>4</sub> aqueous solution while slowly dropping 50 mL of 0.1060 mol L<sup>-1</sup> NaOH aqueous solution in 12 h. In a typical synthesis of Sn@C/graphene nanocomposite, 0.2499 g of GNSs was dispersed in ethylene glycol by ultrasonication. The dispersion was then mixed with the SnO<sub>2</sub> nanoparticles aqueous colloid by stirring and ultrasonication. The solvent of the suspension was separated away by centrifuging. Then the deposition (SnO<sub>2</sub>/graphene) was washed with ethanol for 3 times and dispersed in ethylene glycol again by ultrasonication for 2 h. A hydrothermal process was employed to coat the SnO<sub>2</sub> nanoparticles with carbon using glucose as the carbon source at 180 °C for 12 h, followed by washing with ethanol and drying in vacuum at 55 °C. The obtained powder is SnO<sub>2</sub> nanoparticles coated with carbon and embedded in the graphene (SnO<sub>2</sub>@C/graphene). To get Sn@C/graphene nanocomposite, the obtained SnO<sub>2</sub>@C/graphene powder was reduced at 800 °C for 12 h within a mixture of N<sub>2</sub> (90%)/H<sub>2</sub> (10%) with a flow rate of 50 mL min<sup>-1</sup>.

The structure and morphology of the nanocomposites were analyzed by X-ray diffraction (XRD, Bruker D8 ADVANCE), scanning electron microscopy (SEM, Quanta 200 F), and transmission electron microscopy (TEM, FEI, Tecnai G<sup>2</sup> F30 S-Twin). The carbon content was determined by an element analyzer (Vario EL III).

The electrochemical performance was carried out using the CR2025 coin type cells. In a typical cell, metallic lithium sheet was used as the reference and counter electrode with a microporous polymer separator (Celgard 2325) and liquid electrolyte mixtures containing 1 mol L<sup>-1</sup> LiPF<sub>6</sub> and a solvent mixture of ethylene carbonate (EC) and dimethyl carbonate (DMC) (1:1 by volume) (Beijing Institute of Chemical Reagents, China). The testing electrodes were prepared by coating the slurry, which consists of Sn@C/graphene nanocomposite, polyvinylidene fluoride (PVDF, Kureha, Japan) and acetylene black with a weight ratio of 75:15:10, onto a copper foil. After drying in a vacuum oven at 100 °C the electrodes were punched into circle and assembled in the cell in a Mikrouna (Super-1220) glove box filled with pure argon. The galvanostatical discharge (Li<sup>+</sup> insertion) and charge (Li<sup>+</sup> extraction) were performed with the voltage between 0.01 and 3.0 V vs. Li/Li<sup>+</sup> at the current densities of 100, 300, 500 and 1000 mA g<sup>-1</sup> using a Battery Testing System (Neware

Electronic Co., China). Cyclic voltammetry curves were measured at a scanning rate of 0.2 mV s<sup>-1</sup> within the potential range of 0.01–3.0 V vs. Li/Li<sup>+</sup> using an electrochemistry working station (Zahner IM6ex).

## 3. Results and discussion

XRD patterns of graphene, SnO<sub>2</sub>/graphene and the as-prepared Sn@C/graphene are showed in Fig. 1. The characteristic peaks of SnO<sub>2</sub> (JCPDS no. 41–1445) are found at 26.5°, 33.8°, 51.6° and 60.5° in the patterns of SnO<sub>2</sub>/graphene. The peaks are weak and wide. The average size of the SnO<sub>2</sub> particles calculated by Scherrer equation is about 3 nm. The peaks of Sn@C/graphene are clearly distinguishable and finely corresponding to the tetragonal Sn phase (JCPDS no. 86–2265), demonstrating that the Sn nanoparticles possess high crystallinity. The elemental analysis indicates that the carbon content of the Sn@C/graphene is about 46.87%, which is much higher than the graphene content (about 18.32%) that we added during the preparation. This result proves that after the hydrothermal process, the glucose converts to disordered carbon and the disordered carbon was successfully coated on the composite [6,26].

Fig. 2 presents the images of SEM and TEM of GNSs, SnO<sub>2</sub>/graphene and Sn@C/graphene. Fig. 2a and b presents the representative SEM and TEM images of graphene sheets from the top view, respectively, showing the layered platelets composed of curled nanosheets. This result is in good agreement with that bare graphene sheets showing a weak (0 0 2) diffraction peak in the XRD pattern. The GNSs appear semitransparent and gauze-like, indicating that the GNSs are monolayer or few layers, which is demonstrated by the wrinkled places and the curly edges of the GNSs in the TEM images, as shown in Fig. 2b. Fig. 2c shows that SnO<sub>2</sub> particles are embedded in the GNSs, which are curly and gauze-like. The primary SnO<sub>2</sub> nanoparticles can be observed clearly in Fig. 2e and the size of SnO<sub>2</sub> nanoparticles is about 2–3 nm, which is consistent with the result of XRD. Although some of the primary SnO<sub>2</sub> nanoparticles aggregate to a bigger particle with the size of about 100–200 nm, SnO<sub>2</sub> nanoparticles and the aggregated secondary particles disperse homogeneously on the GNSs (shown in Fig. 2d). After coating with carbon and reduction, the Sn nanoparticles coated with carbon embedded in

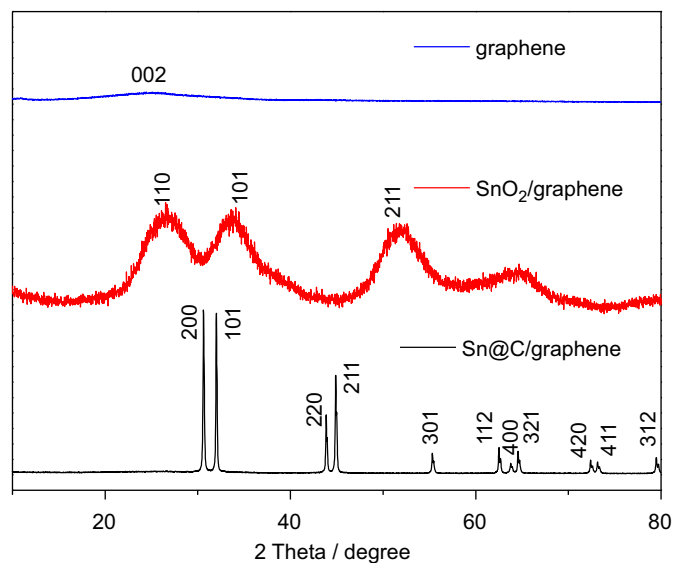
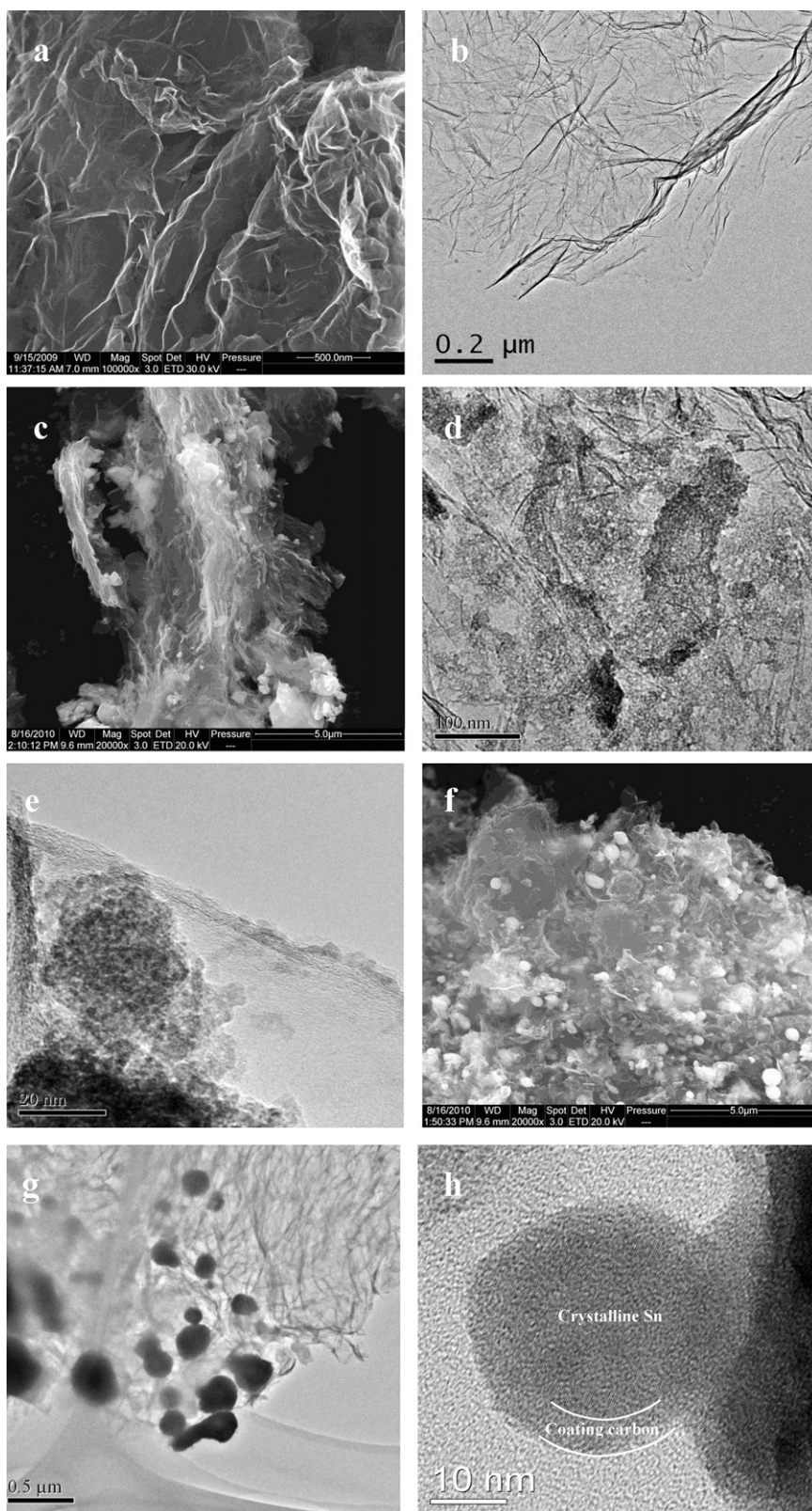


Fig. 1. XRD patterns of graphene, SnO<sub>2</sub>/graphene and the as-prepared Sn@C/graphene.



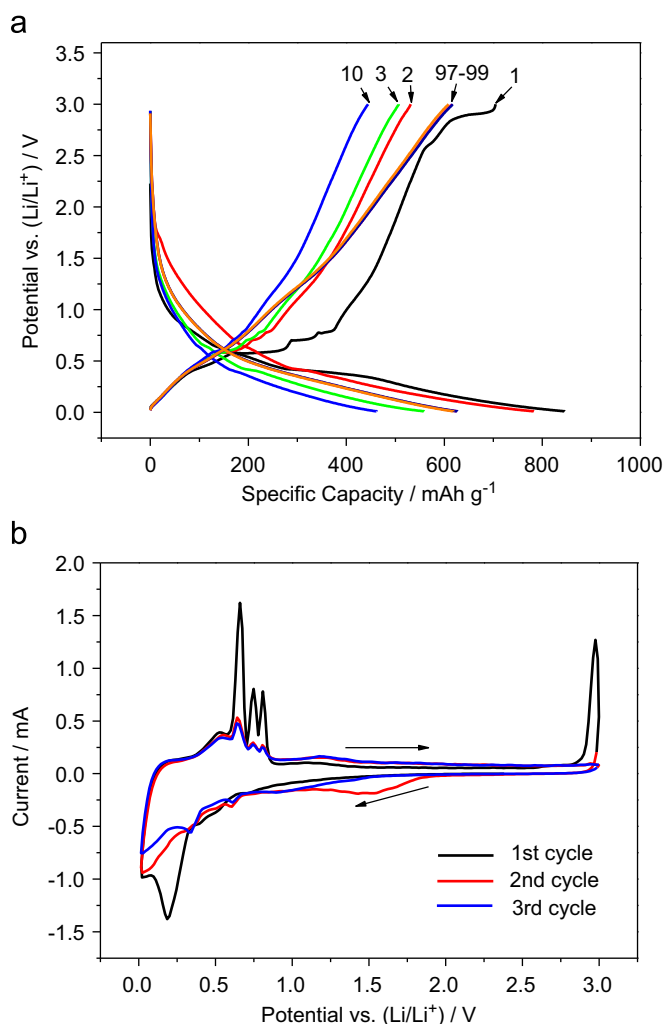
**Fig. 2.** SEM and TEM images of graphene (a and b),  $\text{SnO}_2$ /graphene (c–f) and  $\text{Sn@C}$ /graphene (f–h). The coating carbon and crystalline Sn are marked in (h).

the GNSs are shown in the SEM image of Fig. 2f. The Sn nanoparticles with the diameter of about 50–200 nm are distributed on and between the graphene sheets. The carbon coating (marked in Fig. 2h) decreases the aggregation of the  $\text{SnO}_2$  nanoparticles and wraps up the molten metallic Sn while

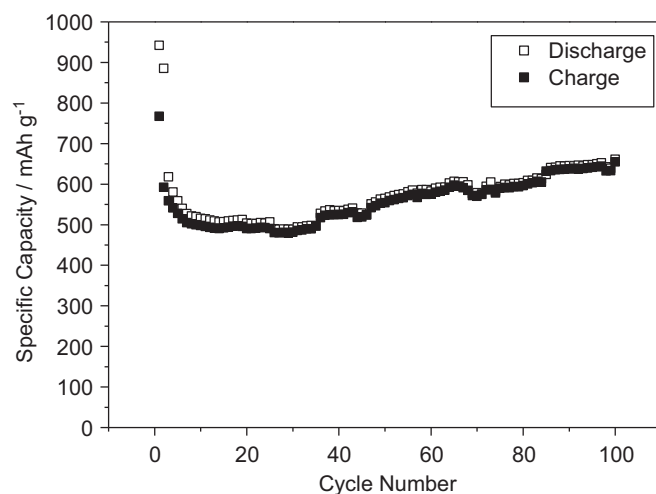
reducing at 800 °C, since the melting point of the metallic Sn is about 232 °C. GNSs contribute to the prevention from aggregation of the nanoparticles and act as current micro-collectors of the  $\text{Sn@C}$  particles due to its high electron conductivity. On the other hand, the curly and wrinkled GNSs stack disordered and form the

porous structure, which create the  $\text{Li}^+$  and electrolyte pathways to the metallic Sn. This specific structure would give an excellent rate capability, which is confirmed by the rate performance tests of the cells.

Galvanostatical discharge ( $\text{Li}^+$  insertion) and charge ( $\text{Li}^+$  extraction) curves are shown in Fig. 3a. All the specific capacities given below are calculated based on the whole Sn@C/graphene nanocomposite. The first cycle curves deliver a high discharge capacity of  $846 \text{ mAh g}^{-1}$  and charge capacity of  $705 \text{ mAh g}^{-1}$ . The initial irreversible capacity can be attributed to the formation of the solid electrolyte interface (SEI) layer and the side reaction of the electrolyte [27]. There are three voltage plateaus clearly observed at 0.6, 0.7 and 0.8 V (vs.  $\text{Li}/\text{Li}^+$ ) corresponding to three steps of the  $\text{Li}^+$  extraction from  $\text{Li}_x\text{Sn}_y$  alloy [28]. The three charge voltage plateaus are characteristic for metallic Sn anode material and correspond to the three intense peaks in the cyclic voltammograms curves shown in Fig. 3b. The overturned humps of the reduction curves of at about 0.2, 0.4 and 0.6 V, are associated to the  $\text{Li}^+$  insertion to the Sn particles [28]. At approximately 2.9 V, there is a broad plateau in the first charge step and an intense peak in cyclic voltammograms curves of the first oxidation cycle, which has not yet been reported in the previous study of metallic Sn as an anode for lithium-ion batteries. This may be ascribed to the secondary reactions of electrolyte anion and the fresh surface of the amorphous carbon, which is loose with plentiful micropore [27,29,30].



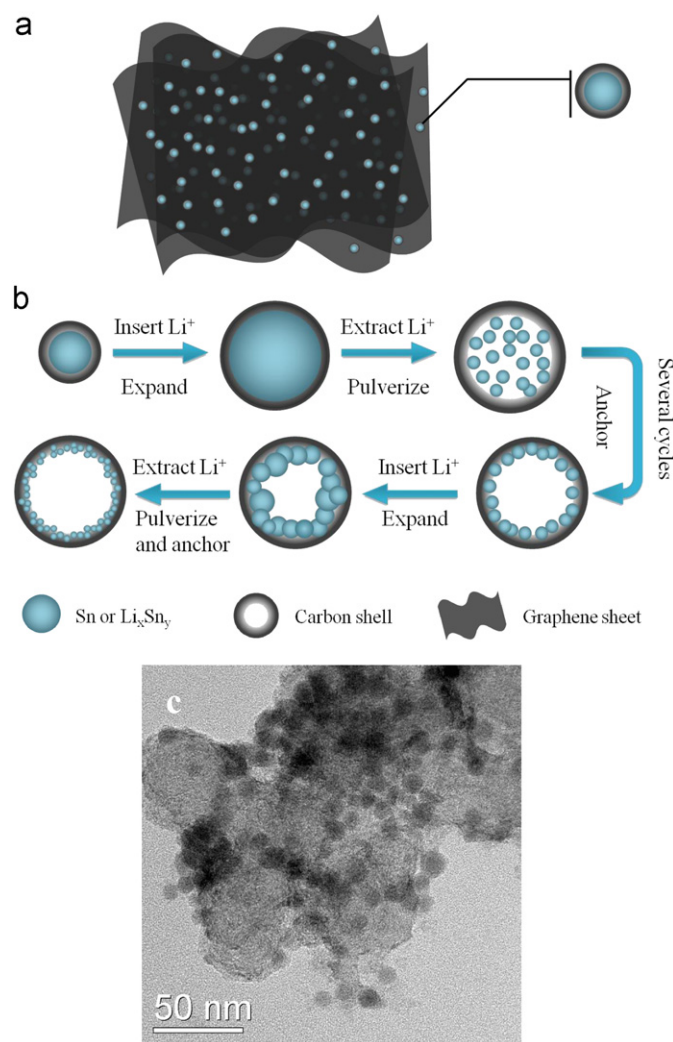
**Fig. 3.** Discharge-charge curves (a) at the specific current of  $100 \text{ mA g}^{-1}$  (the cycle numbers were labeled with arrows) and the cyclic voltammograms (CVs) curves (b) of the Sn@C/graphene nanocomposite.



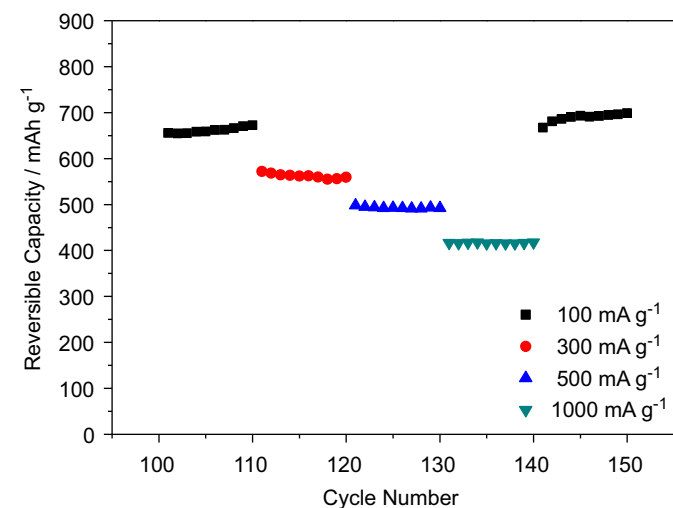
**Fig. 4.** Cycle performance at  $100 \text{ mA g}^{-1}$  of the Sn@C/graphene nanocomposite.

Fig. 4 exhibits that the Sn@C/graphene nanocomposite has a superior cycle performance. Although the capacity fades slowly from the 2nd cycle to the 30th cycle, it increases back and retains at approximately  $660 \text{ mAh g}^{-1}$  after 100 cycles. The phenomenon of firstly decreasing and afterwards increasing of reversible capacity is ascribed to the pulverization of metallic Sn and the buffering effect of the carbon matrix, as shown in Fig. 5. At first, Sn particle and the carbon shell was expanded in the first  $\text{Li}^+$  insertion step [7–9]. The tough and elastic GNSs compensate the large expansion and prevent the carbon shell from cracking. The expanded Sn particle shrinks and is pulverized into small particles when  $\text{Li}^+$  are extracted. However, the rigid carbon shell maintains expanded shape. Therefore, in the initial cycles the pulverized particles do not contact well with each other and with the carbon shell, leading to a poor electric conductivity and capacity fading of the material. Afterwards, because of the electric field force the pulverized Sn particles gradually anchor on the carbon shell leading to a better electronic conductivity and electrochemical activity, which deliver the larger capacity of the nanocomposite during the subsequent charge-discharge cycles. Fig. 5c shows the TEM image of the nanocomposite after being cycled. The carbon shell expanded during cycles and substantial space was left out which is shown in Fig. 5c. The diameter of the pulverized Sn particles is about 6–10 nm, which is much smaller than the pristine Sn particles. The pulverized Sn particles anchored onto the carbon shell and did not drop out even after the ultrasonication of the TEM sample treatment. It is an experimental evidence for the particle expansion, pulverization and the explanation of the superior cycle performance. The superior cycle performance of Sn@C/graphene nanocomposite can be attributed to the synergistic effect of GNSs and carbon coating: (1) GNSs which are tough and elastic enough to compensate the large volume change of the metallic Sn and (2) carbon coating wraps up the pulverized Sn particle and prevents the detachment between the graphene sheets. Compared to the prior reported results of the Sn nanocomposite [19,23], the cycle performance of the electrode material in this study is remarkable and promising for the application of the high performance lithium-ion batteries.

Fig. 6 presents the rate performance of the Sn@C/graphene nanocomposite after 100 cycles at the specific current of  $100 \text{ mA g}^{-1}$ . The charge capacities are 662, 572, 498, 417 and  $699 \text{ mAh g}^{-1}$  at the currents of 100, 300, 500, 1000 and back to  $100 \text{ mA g}^{-1}$ , respectively. Even at the large specific current of  $1000 \text{ mA g}^{-1}$ , the reversible specific capacity still remains 63.0%



**Fig. 5.** Schematic of the Sn@C/graphene nanocomposite (a), the particle expansion and pulverization (b) and the TEM image of the material after being cycled (c). Pulverized Sn particles anchored on the carbon can be observed.



**Fig. 6.** Cycle performance after 100 cycles at 100 mA g<sup>-1</sup> of the Sn@C/graphene nanocomposite.

of that at 100 mA g<sup>-1</sup>. Instead of fading, the specific capacity increases 5.6% when the specific current comes back to 100 mA g<sup>-1</sup>. The excellent rate capability is ascribed to the

pulverized nanoscale Sn particles which shorten the transport lengths for both electrons and lithium ions. Moreover, the curly and wrinkled structure of the GNSs gives a good conductivity of the material.

#### 4. Conclusion

In summary, a novel Sn@C/graphene nanocomposite was synthesized as an anode for lithium-ion batteries. The carbon coating and the specific structure of the graphene matrix can accommodate the volume change during the charge-discharge process of the cells and create the lithium ion and electrolyte pathways inside the electrodes. Therefore, the Sn@C/graphene nanocomposite possesses a large reversible capacity, superior cycle performance (the capacity remains 662 mAh g<sup>-1</sup> at 100 mA g<sup>-1</sup> after 100 cycles and this material delivers no fading but increasing capacity even after the large current cycles) and high rate capability (417 mAh g<sup>-1</sup> at 1000 mA g<sup>-1</sup>). The Sn@C/graphene nanocomposite is promising for the high performance lithium-ion batteries with ultra long life and high energy density.

#### Acknowledgments

This work was financially supported by the National Natural Science Foundation of China (No. 20936001) and the Fundamental Research Funds for the Central Universities, SCUT (2009220038).

#### References

- [1] Y. Idota, T. Kubota, A. Matsufuji, Y. Maekawa, T. Miyasaka, *Science* 276 (1997) 1395.
- [2] J.M. Tarascon, P. Poizot, S. Laruelle, S. Grugeon, L. Dupont, *Nature* 407 (2000) 496.
- [3] A.M. Cao, J.S. Hu, H.P. Liang, L.J. Wan, *Angew. Chem. Int. Ed.* 44 (2005) 4391.
- [4] Y. Wang, J.Y. Lee, H.C. Zeng, *Chem. Mater.* 17 (2005) 3899.
- [5] X.W. Lou, Y. Wang, C. Yuan, J.Y. Lee, L.A. Archer, *Adv. Mater.* 18 (2006) 2325.
- [6] J.S. Chen, Y.L. Cheah, Y.T. Chen, N.J. Jayaprakash, S. Madhavi, Y.H. Yang, X.W. Lou, *J. Phys. Chem. C* 113 (2009) 20504.
- [7] A. Courtney, J.R. Dahn, *J. Electrochem. Soc.* 144 (1997) 2943.
- [8] O. Mao, R.A. Dunlap, J.R. Dahn, *J. Electrochem. Soc.* 146 (1999) 405.
- [9] L.Y. Beaulieu, J.R. Dahn, *J. Electrochem. Soc.* 147 (2000) 3237.
- [10] S.C. Chao, Y.C. Yen, Y.F. Song, Y.M. Chen, H.C. Wu, N.L. Wu, *Electrochem. Commun.* 12 (2010) 234.
- [11] J. Park, J. Eom, H. Kwon, *Electrochem. Commun.* 11 (2009) 596.
- [12] S. Liu, Q. Li, Y. Chen, F. Zhang, *J. Alloy Compd.* 478 (2009) 694.
- [13] M. Noh, Y. Kwon, H. Lee, J. Cho, Y. Kim, M.G. Kim, *Chem. Mater.* 17 (2005) 1926.
- [14] Z. Wang, W. Tian, X. Liu, R. Yang, X. Li, *J. Solid State Chem.* 180 (2007) 3360.
- [15] L. Xue, Z. Fu, Y. Yao, T. Huang, A. Yu, *Electrochim. Acta* 55 (2010) 7310.
- [16] D. Deng, J.Y. Lee, *Angew. Chem.* 48 (2009) 1660.
- [17] R. Li, X. Sun, X. Zhou, M. Cai, X. Sun, *J. Phys. Chem. C* 111 (2007) 9130.
- [18] Y. Yu, Q. Yang, D. Teng, X. Yang, S. Ryu, *Electrochem. Commun.* 12 (2010) 1187.
- [19] W. Zhang, J. Hu, Y. Guo, S. Zheng, L. Zhong, W. Song, L. Wan, *Adv. Mater.* 20 (2008) 1160.
- [20] K.T. Lee, Y.S. Jung, S.M. Oh, *J. Am. Chem. Soc.* 125 (2003) 5652.
- [21] G. Nadeau, X.Y. Song, M. Massé, A. Guerfi, G. Brisard, K. Kinoshita, K. Zaghib, *J. Power Sources* 108 (2002) 86.
- [22] K.S. Novoselov, A.K. Geim, S.V. Morozov, D. Jiang, Y. Zhang, S.V. Dubonons, I.V. Grigorieva, A.A. Firsov, *Science* 306 (2004) 666.
- [23] G. Wang, B. Wang, X. Wang, J. Park, S. Dou, H. Ahn, K. Kim, *J. Mater. Chem.* 19 (2009) 8378.
- [24] W.S. Hummers, R.E. Offeman, *J. Am. Chem. Soc.* 80 (1958) 1339.
- [25] P. Lian, X. Zhu, S. Liang, Z. Li, W. Yang, H. Wang, *Electrochim. Acta* 55 (2010) 3909.
- [26] X. Sun, Y. Li, *Angew. Chem. Int. Ed.* 43 (2004) 597.
- [27] T. Nakajima, V. Gupta, Y. Ohzawa, H. Groult, Z. Mazej, B. Žemva, *J. Power Sources* 137 (2004) 80.
- [28] A. Courtney, J.R. Dahn, *J. Electrochem. Soc.* 144 (1997) 2045.
- [29] Z. Wang, W. Tian, X. Liu, R. Yang, X. Li, *J. Solid State Chem.* 180 (2007) 3360.
- [30] H. Li, L. Shi, W. Lu, X. Huang, L. Chen, *J. Electrochem. Soc.* 148 (2001) A915.